Proceedings

Eighteenth IEEE Symposium on

COMPUTER-BASED MEDICAL SYSTEMS

23–24 June 2005
Dublin, Ireland

Editors
Alexey Tsymbal
Padraig Cunningham

COMPUTER
SOCIETY
IEEE

Special Track 1: Medical Image Analysis: Techniques and Applications

Special Track 2: Intelligent Data Analysis of Electrocardiogram Data

Special Track 3: Data Mining

Special Track 4: Bioinformatics and Its Medical Applications

Special Track 9: Medical Multimedia Analysis and Content-Based Retrieval

Liver	Sens.	Spec.	Prec.	Acc.
Haar (33)	76.92	96.31	73.17	94.07
Haar (99)	71.79	97.99	82.35	94.96
D4 (33 Mirror)	68.42	97.66	78.79	94.36
D4 (99 Mirror)	71.05	97.32	77.14	94.36
C6 (33 Mirror)	57.89	94.31	56.41	90.21
C6 (99 Mirror)	73.68	93.98	60.87	91.69

Kidney	Sens.	Spec.	Prec.	Acc.
	87.50	94.66	76.56	93.47
	85.71	92.88	70.59	91.69
	94.74	89.29	64.29	90.21
	75.44	93.57	70.49	90.50
	64.91	92.86	64.91	88.13
	68.42	92.14	63.93	88.13

Table 4: Classification performance for liver and kidney

Spleen	Sens.	Spec.	Prec.	Acc.
Haar (33)	50.00	98.75	66.67	96.44
Haar (99)	50.00	95.64	36.36	93.47
D4 (33 Mirror)	37.50	99.07	66.67	96.14
D4 (99 Mirror)	25.00	98.13	40.00	94.66
C6 (33 Mirror)	31.25	96.26	29.41	93.18
C6 (99 Mirror)	31.25	96.57	31.25	93.47

Table 5: Classification performance for spleen

10. References

[1] D. Xu, J. Lee, D.S. Raicu, J.D. Furst, D. Channin. "Texture Classification of Normal Tissues in Computed Tomography", The 2005 Annual Meeting of the Society for Computer Applications in Radiology, Orlando, Florida, June 2-5, 2005.

[2] D. Channin, D. S. Raicu, J. D. Furst, D. H. Xu, L. Lilly, C. Limpsangsri, "Classification of Tissues in Computed Tomography using Decision Trees", Poster and Demo, The 90th Scientific Assembly and Annual Meeting of Radiology Society of North America (RSNA04), Chicago, IL, USA, November 28 - December 3rd, 2004.

[3] Kurani, A, Xu, D. H., Furst, J. D., Raicu D. S.. "Co-occurrence matrices for volumetric data", The 7th IASTED International Conference on Computer Graphics and Imaging - CGIM 2004, Kauai, Hawaii, USA, in August 16-18, 2004

[4] D. H. Xu, A. Kurani, J. D. Furst, & D. S. Raicu, "Run-length encoding for volumetric texture", The 4th IASTED International Conference on Visualization, Imaging, and Image Processing - VIIP 2004, Marbella, Spain, September 6-8, 2004.

[5] Kara, Bayram, and Nurdal Watsuji. Using Wavelets For Texture Classification. IJCI Proceedings of International Conference on Signal Processing. ISSN 1304-2386, Column:1, Number: 2. September 2003.

[6] Van de Wouwer, G., P. Scheunders, and D. Van Dyck. Statistical Texture Characterization from Discrete Wavelet Representations. University of Antwerp: Antwerpen, Belgium.

[7] Haralic, R.M., Shapiro, L.G., Computer and Robot Vision, Addison_wesley Publishing Co., 1992.

Computer-Aided Thyroid Nodule Detection in Ultrasound Images

D.E. Maroulis[a], M.A. Savelonas[a], S.A. Karkanis[b], D.K. Iakovidis[a], N. Dimitropoulos[c]
[a]Dept. of Informatics and Telecommunication, University of Athens, Greece
[b]Dept. of Informatics and Computer Technology, Technological Educational Institute of Lamia, Greece
[c]Dept. of Medical Imaging, Euromedica Medical Center, Athens, Greece
rtsimage@di.uoa.gr

Abstract

Nodular thyroid disease is a frequent occurrence in clinical practice and it is associated with increased risk of thyroid cancer and hyperfunction. In this paper we propose a novel method for computer-aided detection of thyroid nodules in ultrasound (US) images. The proposed method is based on a level-set image segmentation approach that takes into account the inhomogeneity of the US images. This novel method was experimentally evaluated using US images acquired from 35 patients. The results show that the proposed method achieves more accurate delineation of the thyroid nodules in the US images and faster convergence than other relevant methods.

1. Introduction

Nodular thyroid disease is extremely common and of concern because of the risk of malignancy and hyperfunction. The risk of developing a palpable thyroid nodule in a lifetime ranges between 5 and 10%, while 50% of people with solitary nodules detected by experienced physicians have additional nodules detected when examined further by ultrasonography [1].

Thyroid ultrasonography is a non-invasive diagnostic test, which provides immediate information on the structure and the characteristics of thyroid nodules. It combines low cost, short acquisition time, absence of ionizing radiations and sensitivity in ascertaining the size and number of thyroid nodules. However ultrasound (US) images contain echo perturbations and speckle noise, which could make the diagnostic task harder. Additionally, image interpretation, as performed by the experts, is subjective. Therefore, a method for computer-aided thyroid nodule detection should take into consideration the inherent noise characteristics of the US images and be capable of interpreting these images, based on explicit image features. Such a method could contribute to the objectification of the medical diagnosis and consequently to a reduction of false decisions.

Active contour models first appeared in the late eighties [2]. The classic active contour approach in image segmentation is based on the deformation of initial contours towards the boundaries of the image regions to be segmented. The deformation is realized by the minimization of an energy functional designed so that its local minimum is reached at the target boundaries. The energy functional in its basic form is comprised of two components, the first controls the smoothness of the contour and the second is image dependent and forces the contour towards the boundary. This active contour approach is boundary based and utilizes local filtering techniques such as edge detection operators. In the case of noisy images, such as US images, many unwanted edges may appear due to noise, and should consequently be smoothed by the application of a strong isotropic Gaussian filter. Such filtering introduces the risk of smoothing the target boundaries and therefore contour leakage effects may appear resulting in diminution of the delineation accuracy [3]. Moreover, the

parametric formulation of the classic active contour approach, does not allow for changes in the topology of the evolving contour, such as splitting and merging. Therefore, complementary procedures have to be considered to enable adaptability to the required topological changes [4].

Active contours have been employed in various medical US image analysis applications either in parametric or in level set form. Parametric active contour applications include the detection of hepatic tumors [5], the detection of lumen and media-adventitia border in sequential intravascular ultrasound (IVUS) frames [6] and the evaluation of margins for malignant breast tumor excision through mammotomes [7]. Level set active contour applications include the automatic quantification of the ventricular function [8] and the segmentation of prostate [9] and cardiac US images [10]. To the best of our knowledge there has not been proposed any information technology approach to thyroid nodule detection in US images.

Active Contours Without Edges (ACWE) [3] has been proposed as a noise-robust image segmentation method. It is capable of detecting objects even with smooth boundaries due to its region-based approach in which the functional is a combination of domain and boundary integrals. Moreover, following the level set formulation, originally proposed in [11], it is capable of detecting two or more objects in the image as it provides adaptability to topological changes e.g. contour splitting. A limitation of this model is that it presumes homogeneity for object and background areas. This presumption is violated in thyroid US images due to the intensity inhomogeneity of the thyroid tissue texture and the presence of calcifications appearing in the form of bright spots. A modification that takes into account image inhomogeneity could lead to more accurate object detection.

In this paper, we propose a novel level set active contour model, for thyroid nodule detection in US images that takes into account image inhomogeneity by utilizing a variable background approach for the enhancement of the nodule detection accuracy while achieving faster contour convergence.

The rest of this paper is organized in three sections. Section 2 includes a brief description of the Active Contour Without Edges model and the presentation of the proposed Variable Background Active Contour model. The experimental results from the application of the proposed model on thyroid ultrasound images are apposed in Section 3. Finally, Section 4 summarizes the conclusions of this study.

2. Variable Background Active Contour Model

2.1. Active Contour Without Edges

The ACWE model as posed in [3] has the form of a minimization problem: Let Ω be a bounded open subset of R^2 and $\partial\Omega$ its boundary. We seek for $\inf F(c^+, c^-, C)$,

$$F(c^+, c^-, C) = \mu \cdot Length(C)$$
$$+ \lambda^+ \int_{inside(C)} |u_0(x,y) - c^+|^2 \, dxdy \qquad (1)$$
$$+ \lambda^- \int_{outside(C)} |u_0(x,y) - c^-|^2 \, dxdy$$

where $u_0 : \Omega \to R$ is the input image, $C(s) : [0,1] \to R^2$ a piecewise parameterized curve, c^+ and c^- are unknown constants representing the average value of u_0 inside and outside the curve and parameters $\mu > 0$ and $\lambda^+, \lambda^- > 0$ are weights for the regularizing

term and the fitting terms, respectively. This formulation describes a special case of the minimal partition problem, for which the existence of minimizers has been proved in [12] for u_0 continuous on Ω and in [13] for more general data. As in the minimum energy problem, the minimizer corresponds to the "equilibrium" of the regularizing and fitting terms that force the contour to stop. It should be noted that, as implied by (1), this model assumes that the image is formed by two regions of approximately piecewise constant intensities.

In the level set method [11], $C \subset \Omega$ is represented by the zero level set of a Lipschitz function $\phi : \Omega \to R$, such that

$$C = \{(x,y) \in \Omega : \phi(x,y) = 0\},$$
$$inside(C) = \{(x,y) \in \Omega : \phi(x,y) > 0\}, \qquad (2)$$
$$outside(C) = \{(x,y) \in \phi(x,y) < 0\}$$

Using the one-dimensional Dirac measure δ and the Heaviside function H, which are defined respectively by

$$\delta(z) = \frac{d}{dz} H(z) \quad H(z) = \begin{cases} 1, & if \ z \geq 0 \\ 0, & if \ z < 0 \end{cases} \qquad (3)$$

where $z \in R$, the constants c^+ and c^- can be expressed as

$$c^+(\phi) = \frac{\int_\Omega u_0(x,y) H(\phi(x,y)) dxdy}{\int_\Omega H(\phi(x,y)) dxdy} \qquad (4)$$

$$c^-(\phi) = \frac{\int_\Omega u_0(x,y)(1 - H(\phi(x,y))) dxdy}{\int_\Omega (1 - H(\phi(x,y))) dxdy} \qquad (5)$$

By keeping c^+ and c^- fixed, and minimizing F with respect to ϕ, the associated Euler-Langrange equation for ϕ is deduced. For this purpose, slightly regularized versions of H and δ are considered. The applied $C^\infty(\overline{\Omega})$ regularized Heaviside function H_ε is derived from

$$H_\varepsilon = \frac{1}{2} \cdot (1 + \frac{2}{\pi} \arctan(\frac{z}{\varepsilon})) \qquad (6)$$

whereas the corresponding regularized delta function δ_ε is derived from $\delta_\varepsilon = dH_\varepsilon / dz$. As $\varepsilon \to 0$, both approximations converge to H and δ. These approximations allow the algorithm to compute a global minimizer, as described in [3].

Parameterizing the descent direction by an artificial time $t \geq 0$, the equation in $\phi(t,x,y)$ (with $\phi(0,x,y) = \phi_0(x,y)$ defining the initial contour) is

$$\frac{\partial \phi}{\partial t} = \delta(\phi)[\mu \cdot div(\frac{\nabla \phi}{|\nabla \phi|}) - \lambda^+ (u_0 - c^+)^2 + \lambda^- (u_0 - c^-)^2] = 0 \qquad (7)$$

where $t \in (0, \infty), (x, y) \in \Omega$.

In a practical implementation, a quantitative criterion should force the algorithm to stop when the changes of ϕ fall bellow a threshold for a fixed number of iterations. When this criterion is satisfied it is assumed that the minimizer is found and the corresponding equilibrium has been reached.

2.2. Variable Background Active Contour

The proposed model, named Variable Background Active Contour (VBAC) follows Eq. (1) where c^- is derived from Eq. (8):

$$c^-(\phi) = \frac{\int_\Omega u_0(x,y)(1 - H(\phi(x,y)))H(\phi_0(x,y))\Delta(x,y)dxdy}{\int_\Omega (1 - H(\phi(x,y)))H(\phi_0(x,y))\Delta(x,y)dxdy} \qquad (8)$$

and the difference term $\Delta(x, y)$ is given by:

$$\Delta(x,y) = H(\phi(x,y) - a) - H(\phi(x,y)), \quad a > 0 \qquad (9)$$

Note that $H(\phi_0)$ restricts the integrals in a region of interest, which for the purposes of our study coincides with the thyroid gland. The constant a, determines the background area considered. The introduction of $\Delta(x, y)$ reduces the effects of background area inhomogeneities corresponding to calcifications appearing in the US image in the form of bright spots as well as to the intensity inhomogeneity of the thyroid tissue texture. This can be justified by the fact that these inhomogeneities cause abrupt changes of ϕ which result in $H(\phi(x,y) - a) = H(\phi(x,y)) = 1$ for the inhomogeneous areas in the image. Therefore, $\Delta(x, y) \neq 0$ is satisfied in a limited image subset, which excludes inhomogeneous areas.

3. Results

Thyroid ultrasound examinations were performed on 35 patients using a digital ultrasound system HDI 3000 ATL with a 5-12 MHz linear transducer. The acquired digital images had a resolution of 256×256 pixels and 256 gray-level depth. We developed a special purpose software suite in Microsoft Visual C++ for the implementation of the ACWE and the VBAC models. Both of these models were applied for thyroid nodule detection in the US images using $\lambda^+ = 5$, $\lambda^- = 5$, $\mu = 650$ and $a = 10^{-13}$. For the purposes of our study we adopted the image intensity as the supervising feature for the contour evolution, to enable the detection of hypo-echoic thyroid nodules. Low echogenicity characterizes the majority of thyroid nodules and especially those that are suspect of malignancy [14].

Three expert radiologists manually delineated the thyroid nodules to enable comparisons with the active contour models. For each US image, "ground truth" delineation is obtained, following the rule that each pixel is considered as part of the nodule when it is included in at least two out of three experts' delineations [15]. As a measure of similarity between a delineated area A and the "ground truth" delineated area G, we have considered the overlap value [16]:

$$i = \frac{A \cap G}{A \cup G} \qquad (10)$$

The inter observer variation was estimated 7.4% in terms of the Coefficient of Variation $CV\% = 100 \cdot (\sigma_i / m_i)$, where σ_i and m_i are the standard deviation and the mean value of i, respectively [15].

The experiments showed that the proposed VBAC model and the ACWE model converged to overlap values with an average difference of $\Delta i = i_{VBAC} - i_{ACWE} = 6.2 \pm 2.3\%$. Both models resulted in a maximum overlap of 99.1%. The minimum overlap values obtained were 78.6% and 62.1% for the VBAC and the ACWE models respectively, whereas the corresponding mean overlap values were 88.8% and 82.6%. Moreover with the VBAC model corresponding mean overlap values were 88.8% and 82.6%. Moreover with the VBAC model the convergence was reached in 10% less algorithm iterations than with the ACWE model, which is translated in approximately 8.5% speedup in terms of absolute execution time.

Figure 1 illustrates an example US image delineated by an expert radiologist, the VBAC and the ACWE models respectively. It can be observed that the VBAC surrounded the hypo-echoic nodule more accurately than the ACWE compared to the expert's delineation. The overlap values achieved per iteration for the image of Fig. 1 are illustrated in Fig. 2. This figure shows that the VBAC model converges to a higher overlap value (94.6%) in approximately 10^3 less iterations than the ACWE model which leads to a maximum overlap value of 80.9%.
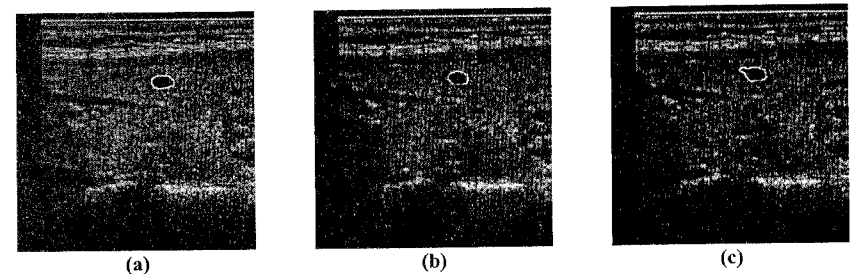

| (a) | (b) | (c) |

Figure 1. Two indicative examples of a thyroid nodule in a US image delineated by (a) an expert radiologist, (b) the VBAC, and (c) the ACWE.
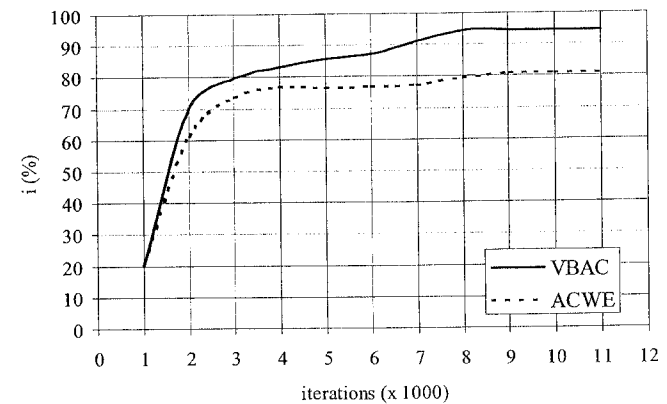

Figure 2. Overlap value i as a function of the number of algorithm iterations corresponding to the US image illustrated in Fig. 1, using the ACWE and the VBAC models.

4. Conclusion

We have proposed a Variable Background Active Contour model and applied it for the detection of thyroid nodules in ultrasound images. In this model, the background is a variable subset of the image, which changes shape to reduce the effects of background inhomogeneity. The results of the experimental study lead to the conclusion that the proposed model provides improved accuracy and faster convergence, compared to the Active Contour Without Edges model. In particular, the improvement in contour accuracy is important due to the fact that nodule size and shape are factors affecting the subsequent nodule classification [1].

Future perspectives of this work include the embedment of textural features to supervise contour evolution enabling the detection of non hypo-echoic nodules.

5. Acknowledgments

6. References

[1] S. Feld et all, "AACE Clinical Practice Guidelines for the Diagnosis and Management of Thyroid Nodules", Endocrine Practice, Jan./Feb. 1996, pp. 78-84.

[2] W. Kass, A. Witkin, D. Terzopoulos, "Snakes: Active Contour Models", Int. J. Comput. Vision, vol. 1, no. 4, 1987, pp. 321-331.

[3] T.F. Chan, L.A. Vesse, "Active Contours Without Edges", IEEE Trans. Image Processing, Feb. 2001, pp. 266-277.

[4] T. McInerney, D. Terzopoulos, "Topologically Adaptable Snakes", Proc. Int. Conf. Comp. Vis., Cambridge, Jun. 1995, pp. 840-845.

[5] C.M. Chen, H.H.S Lu, A.T. Hsiao, "A Dual-Snake Model of High Penetrability for Ultrasound Image Boundary Extraction", Ultrasound in Med. & Biol., vol.27, no.12, 2001, pp. 1651-1665.

[6] M.E. Plissiti, D.I. Fotiadis, L.K. Michalis, G.E. Bozios, "An Automated Method for Lumen and Media-Adventitia Border Detection in a Sequence of IVUS Frames", IEEE Trans. On Inf. Tec. in Biomedicine, vol. 8, no. 2, Jun. 2004, pp. 131-141.

[7] R.F. Chang, W.J. Wu, C.C. Tseng, D.R. Chen, W.K. Moon, " 3-D Snake for US in Margin Evaluation for Malignant Breast Tumor Excision Using Mammotome", IEEE Trans. On Inf. Tec. in Biomedicine, vol. 7, no. 3, Sep. 2003.

[8] E. Angelini, J. Holmes, A. Laine, "Segmentation of RT3D Ultrasound with Implicit Deformable Models Without Gradients", Proc. ISPA 2003, Rome, Italy, Sep. 2003, Part II, pp. 711-716.

[9] D. Honigmann, J. Ruisz, and H. Pottmann, "Fast Model Based Segmentation of Ultrasound Data using an Active Image", Proc. IEEE Int. Symp. on Biomedical Imaging, Washington DC, 2002, pp. 225-228.

[10] N. Lin, W. Yu, J.S. Duncan, "Combinative Multi-scale Level Set Framework for Echocardiographic Image Segmentation", Medical Image Analysis, vol. 7, 2003, pp. 529-537.

[11] S. Osher, J. Sethian, "Fronts Propagating with Curvature- Dependent Speed: Algorithms Based on the Hamilton-Jacobi Formulations", Journal Of Computational Physics, vol. 79, 1988, pp.12-49.

[12] D. Mumford, J. Shah, "Optimal Approximation by Piecewise Smooth Functions and Associated Variational Problems", Commun.Pure Appl. Math., vol.42, 1989, pp 577-685.

[13] J.M. Morrel, S. Solimini, "Segmentation of Images by Variational Methods: A Constructive Approach", Madrid, Spain: Revista Matematica Universidad Computense de Madrid, vol.1, 1988, pp.169-182.

[14] E. Papini et al, "Risk of Malignancy in Nonpalpable Thyroid Nodules: Predictive Value of Ultrasound and Color-Doppler Features", The Journal of Clinical Endocrinology & Metabolism, vol. 87, no.5, 2002, pp. 1941-1946.

[15] M.R. Kaus, S.K. Warfield, F.A. Jolesz, R. Kikinis, "Segmentation of Meningiomas and Low Grade Gliomas in MRI", Proc. Second International Conference on Medical Image Computing and Computer-Assisted Intervention, Cambridge, England, 1999, pp. 1-10.

[16] X. Hao, C. Bruce, C. Pislaru and J.F. Greeneaf, "A Novel Region Growing Method for segmenting ultrasound images", IEEE International Ultrasonics Symposium, Oct. 2000.

A Comparative Study of Texture Features for the Discrimination of Gastric Polyps in Endoscopic Video

D.K. Iakovidis[a], D.E. Maroulis[a], S.A. Karkanis[b], A. Brokos[a]

[a]Dept. of Informatics and Telecommunications, University of Athens, Greece
[b]Dept. of Informatics and Computer Technology, Technological Educational Institute
of Lamia, Greece
rtsimage@di.uoa.gr

Abstract

In this paper, we extend the application of four texture feature extraction methods proposed for the detection of colorectal lesions, into the discrimination of gastric polyps in endoscopic video. Support Vector Machines have been utilized for the texture classification task. The polyp discrimination performance of the surveyed schemes is compared by means of Receiver Operating Characteristics (ROC). The results advocate the feasibility of a computer-based system for polyp detection in video gastroscopy that exploits the textural characteristics of the gastric mucosa in conjunction with its color appearance.

1. Introduction

Gastric cancer is the second most common cancer-related cause of death in the world [1]. Its symptoms are rarely alarming until late stages, and as a result they are usually ignored by the patients. Furthermore, over 40% of gastric malignancies appear as polyps. However, over the past 20 years, there has been a significant increase in survival rates, which is mainly due to the earlier detection of cancer precursors through screening and thorough symptom investigation. Standard video gastroscopy remains the most efficient minimally invasive procedure to detect even small-size lesions that allows biopsy and in many cases polyp resection [1]. A reliable system that would be capable of supporting the detection of gastric polyps could increase the endoscopist's ability to accurately locate them, and could contribute to the reduction of the duration of the endoscopic procedure, which discomforts the patients. Moreover, such a system would minimize the expert's subjectivity introduced in the evaluation of the clinical characteristics of the examined tissue.

Computer-based approaches that have been proposed in the literature for the discrimination of abnormal conditions of the gastric tract include the employment of edge detection methods for the detection of gastric ulcers [2] and the diagnosis of gastric carcinoma via classification of epidemiological data [3]. To the best of our knowledge, there has been no previous study regarding computer-based discrimination of gastric polyps in endoscopic video yet.

In this work, we investigate the appropriateness of four texture feature extraction methods proposed in the recent literature for the discrimination of colorectal lesions in endoscopic images or video, for the discrimination of gastric polyps. Namely, the surveyed schemes are the Color Wavelet Covariance [4], the Texture Spectrum Histogram [5][6], the Texture Spectrum and Color Histogram Statistics [7], and the Local Binary Pattern [8]. The classification task is assigned to Support Vector Machines (SVMs), as these have proven robust, resistant to the "curse of dimensionality" and suitable for texture classification [9].

The rest of this paper is organized in three sections. Section 2 describes the feature extraction methods used. In section 3, we appose the experimental results on the performance of the feature extraction methods for the discrimination of polyps from normal. Finally, the conclusions of this study are summarized in Section 4.

2. Feature Extraction Methods

2.1. Texture Spectrum Histogram

The Texture Spectrum (TS) method has been proposed by Wang and He [10] and it is based on texture units which characterize the local texture information for a given pixel and its neighborhood. This scheme analyzes an image in the following way:

a) A 3×3 neighborhood of pixels is thresholded into three levels (0, 1 and 2) using the value of the center pixel. Representing the intensity value of the central pixel as V_0 and the intensity value of each neighboring pixel as V_i, the texture unit is defined as: $TU = \{E_1, E_2, ..., E_8\}$, where

$$E_i = \begin{cases} 0 & if \quad V_i < V_0 \\ 1 & if \quad V_i = V_0 \\ 2 & if \quad V_i > V_0 \end{cases} \tag{1}$$

for $i = 1, 2, ..., 8$. Each element of the TU has one of three possible values; therefore the combination of all the eight elements results in $3^8 = 6561$ possible TU's in total.

b) The values E_i in the thresholded neighborhood are multiplied by certain weights assigned to the corresponding pixels and are summed to obtain a single texture unit number N_{TU} for the corresponding pattern, using the following equation:

$$N_{TU} = \sum_{i=1}^{8} E_i \times 3^{i-1} \tag{2}$$

c) The above procedure is applied to all 3×3 neighborhoods, thus forming the texture spectrum distribution.

2.2. Texture Spectrum and Color Histogram Statistics

The Texture Spectrum and Color Histogram Statistics (TSCHS) method has been proposed by Tjoa and Krishnan [7] and utilizes statistical measures in order to provide an abstract representation of the texture spectrum histogram, applied on various image components C, such as intensity, hue and saturation. Once the histogram has been created, six statistical measures are utilized for its approximation, namely energy, mean, standard deviation, skew, kurtosis and entropy.

In addition, the output vector is complemented by separate color features, as gastrointestinal tumors exhibit exploitable color information [11]. For each image component C, certain lower L_1 and upper threshold L_2 values of the histogram of the regions of interest are selected. The color features β_C are defined as follows:

$$\beta_C = \sum_{i=L_1}^{L_2} Hist_C(i) \Big/ \sum_{i=0}^{L-1} Hist_C(i) \tag{3}$$

where $Hist_C(i)$ is the histogram amplitude at level i of a particular color component C, and L is the total number of levels considered.

2.3. Local Binary Pattern Histogram

The Local Binary Pattern (LBP) method has been proposed by Ojala et al [12] as a two-level version of the texture spectrum method which uses two levels for the representation of local texture patterns. The LBP values are calculated as follows:

$$E_i' = \begin{cases} 0 & if \quad V_i < V_0 \\ 1 & if \quad V_i \geq V_0 \end{cases} \tag{4}$$

$$LBP = \sum_{i=1}^{8} E_i' \times 2^{i-1} \tag{5}$$

The feature vectors are formed by the histogram bins of the LBP values distribution in an image region. The LBP method utilizes $2^8 = 256$ possible texture units instead of the 6561 units utilized in the TS method, leading to a more efficient representation of texture.

2.4. Color Wavelet Covariance

The Color Wavelet Covariance (CWC) features have originally been proposed as covariance estimates of the 2nd order statistical information inherent in the Discrete Wavelet Transform (DWT) of the color components of an image [4]. In this paper, instead of the standard DWT we employ the Discrete Wavelet Frame Transform (DWFT) which tends to decrease the variability of the estimated texture features and it results in a texture characterization invariant under translation [13].

The estimation of the CWC features requires that K-level DWFT is applied to each color component of the image. The 2nd-order statistical information of the wavelet coefficients is captured by means of co-occurrence matrices. Let $M_{C_i}^{B_j(k)}(a)$ be a co-occurrence matrix estimated over a detail image $B_j(k)$, $j = 1, 2, 3$, $k = 1, 2, ... K$ level of DWFT, of the color component C_i, $i = 1, 2, 3$, for a direction $a \in \{0, \pi/4, \pi/2, 3\pi/4\}$. Four representative statistical features are estimated over each detail image, namely the angular second moment, the correlation, the inverse difference moment and the entropy. The Color Wavelet Covariance of a Feature F, between the detail images $B_j(k)$ of the color components C_l and C_m, $l = 1, 2, 3$, $m = 1, 2, 3$ is estimated by the following equation:

$$CWC_{C_i,C_m}^{B_j(k)} = Cov\left(F_{C_i}^{B_j(k)}, F_{C_m}^{B_j(k)}\right), l \leq m \tag{6}$$

3. Results

The experimental evaluation of the four feature extraction methods presented in this paper aims to determine the most suitable feature set for the discrimination of gastric polyps from normal tissues in gastroscopic videos. Only adenomatous polyps have been considered in our study as the probability of them evolving into malignant tumors is higher than that of other polyps [14]. The average size of the polyps examined was 14mm. The videos were acquired with a standard gastroscope and were digitized at a 320×240-pixel resolution, which is supported by most conventional video frame grabbing devices. From each frame a 128×128-pixel region of interest was considered so as to capture only the useful part (dotted line in Fig. 1) of each gastroscopic video frame. We have focused on the use of low rather than high resolution videos, aiming to investigate the feasibility of a low-cost computer-based medical system, which combines both short processing times and bandwidth requirements, and thus it is potentially applicable in telemedicine applications.

Expert gastroscopists selected 1000 representative video frames, containing mostly close-up views of polyps and normal tissues, from which a total of 4000 non-overlapping sub-images of 32×32-pixel size was extracted. In the 128×128-pixel images it was quite difficult to find regions larger than 32×32-pixels which contain only abnormal tissues. Moreover, as most of the feature extraction methods used are based on statistics, the larger the population

of pixels in the sub-image, the most informative the features are expected to be. So, half of the sub-images were acquired from image regions of verified normal tissues while the rest half were acquired from image regions of verified polyp tissues. Moreover, sub-images from dark image regions or regions of strong light reflections have not been included in the dataset because the textural characteristics of the corresponding tissues are either extenuated or distorted.
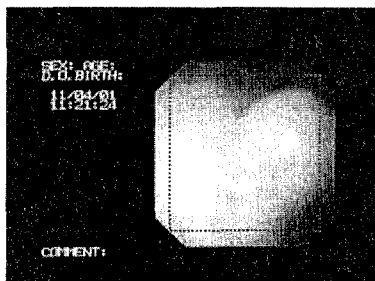

Figure 1. A raw video frame as acquired from the gastroscope

An example gastroscopic video frame sequence is presented in Fig. 2. The first three images (a-c) illustrate a benign-appearing malignant gastric polyp captured in a close-up view, whereas the larger part of the fourth image (d) illustrates normal gastric mucosa. The square regions marked on the video frames indicate sample sub-images that correspond to verified abnormal (a-c) and normal gastric tissues (d).

The TS and LBP feature extraction methods were applied only on the intensity image component. The TSCHS and the CWC schemes were applied on color spaces that have led to optimum performance in earlier studies [4][7]. Namely, these color spaces are the HSI and the $I_1I_2I_3$ respectively.

(a)   (b)   (c)   (d)
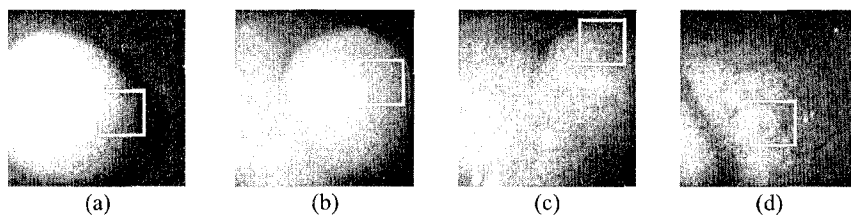
Figure 2. Gastroscopic video frame sequence. The squares indicate sample sub-images corresponding to abnormal (a-c) or normal (d) tissues

Sample classification was realized using the Gaussian kernel-SVM. The Gaussian kernel usually has better boundary response as it allows for extrapolation, and most high-dimensional data sets can be approximated by Gaussian-like distributions similar to those used by RBF networks [15]. In accordance with the recommendation in reference [16] 10-fold cross validation was performed for the production of Receiver Operating Characteristics (ROCs) and average Areas Under Characteristics (AUCs) were obtained. The resulting ROCs are illustrated in Fig. 3. The estimated average AUC for each feature extraction method is 75.2±2.6% for the TS, 80.6±2.5% for the LBP, 87.5±2.1% for the TSCHS and 88.6±2.3% for the CWC method.
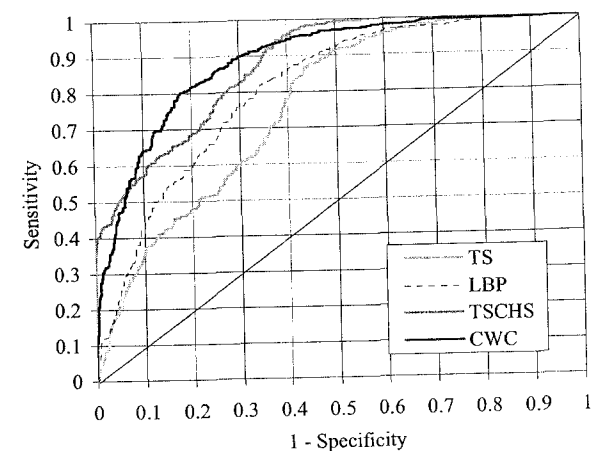

Figure 3. ROC curves obtained using various feature extraction methods

4. Conclusions

We have considered texture as a primary discriminative feature of gastric polyps. Four texture features that have been proposed in the literature for the discrimination of colonic lesions were utilized for the discrimination of gastric polyps, and their performance was compared by means of ROC analysis. The results show that the development of a computer-based medical system using texture features for the detection of gastric polyps is feasible. Moreover, color information, encoded either jointly or separately in the feature vectors, enhances gastric polyp discrimination. The performances of the spatial and of the wavelet domain color texture features employed are comparable.

5. Acknowledgments

6. References

[1] A. M. Desai, M. Preek, P. G Nightingale, and J. W. Fielding, "Improving Outcomes in Gastric Cancer over 20 Years", Gastric Cancer, Springer Verlang Tokyo Inc, 2004, pp. 196-203.

[2] H. Kodama, F. Yano, S. P. Ninomija, Y. Sakai, and S. Ninomija, "A Digital Imaging Processing Method for Gastric Endoscope Picture", in Proc. 21st Annual Hawaian International Conference on System Sciences, 1988, vol. 4, pp. 277-282.

[3] H. A. Güvenir, N. Emeksiz, N. Ikizler, and N. Örmeci, "Diagnosis of Gastric Carcinoma by Classification on Feature Projections," Artificial Intelligence in Medicine, 2004, vol 31, pp. 231-240.

[4] S. A. Karkanis, D. K. Iakovidis, D. E. Maroulis, D. A. Karras, and M. Tzivras, "Computer Aided Tumor Detection in Endoscopic Video using Color Wavelet Features", IEEE Transactions on Information Technology in Biomedicine, vol. 7, 2003, pp. 141-152.

[5] S. Karkanis, K. Galousi, and D. Maroulis, "Classification of endoscopic images based on texture spectrum", in Proc. Workshop on Machine Learning in Medical Applications, Advance Course in Artificial Intelligence, 1999, pp. 63-69.

[6] V. Kodogiannis, and H.S. Chowdrey, "Multi network classification scheme for computer-aided diagnosis in clinical endoscopy", in Proc. MEDSIP 2004 - Int. Conference on Advances in Medical Signal and Information Processing, Malta, 2004, pp. 262-267.

[7] M. P. Tjoa, and S. M. Krishnan, "Feature Extraction for the Analysis of Colon Status from the Endoscopic Images", Biomedical Engineering Online, 2003, pp. 2-9.

[8] M. M. Zheng, S. M. Krishnan, and M. P. Tjoa, "A fusion-based clinical decision support for disease diagnosis from endoscopic images", Computers in Biology and Medicine, 2005, vol. 35, pp. 259-274.

[9] S. Li, J. T. Kwok, H. Zhu, and Y. Wang, "Texture Classification using the Support Vector Machines", Pattern Recognition, vol. 36, pp. 2883-2893, 2003.

[10] L. Wang, and D.C. He, "Texture Classification Using Texture Spectrum", Pattern Recognition, vol 23, 1990, pp. 905-910.

[11] H. Kato, and J. P. Barron, "Electronic Videoendoscopy", Japan: Harwood Academic Publisher, 1993.

[12] T. Ojala, and M. Pietikäinen, "Unsupervised Texture Segmentation using Feature Distributions", Pattern Recognition, 1998, vol. 32, pp. 477-486.

[13] M. Unser, "Texture Classification and Segmentation Using Wavelet Frames", IEEE Trans. on Image Processing, vol. 4, no. 11, 1995.

[14] S. H. Itzkowitz, Y. S. Kim, "Sleisinger & Fordtran's Gastrointestinal and Liver Disease", 6th ed., vol. 2, Philadelphia, WB Saunders Company, 1998.

[15] C. Burges, "A Tutorial on Support Vector Machines for Pattern Recognition", Kluwer Academic Publishers 1998.

[16] A. P. Bradley, "The Use of The Area Under the ROC Curve in the Evaluation of Machine Learning Algorithms", Pattern Recognition, 1997, vol. 30, no. 7, pp. 1145-1159.